SLAC-TN-05-019

LCLS TN 04-4
April 2004

Design Considerations for the LCLS RF Gun

R. Boyce, D.H. Dowell, J. Hodgson, J.F. Schmerge, N. Yu
Stanford Linear Accelerator Center

Abstract

The LCLS rf gun design requires several modifications from existing S-band rf guns. The modifications that have the largest impact on the design of the gun are a dual rf feed and additional cooling capacity for 120 Hz operation. A list of electrical and mechanical specifications have been developed to produce the desired rf field. The simulation code ANSYS was used to study the steady state thermal properties of a 120 Hz gun. It was determined that four cooling channels at appropriate locations could be used to maintain the gun at a nearly constant frequency. The gun body stresses were all at or below the yield strength of Cu except for at the rf apertures. The stress at the apertures is over twice the yield strength and additional work is necessary to reduce the stress and still produce the desired rf coupling coefficient. Only steady state temperatures were calculated and no pulsed heating effects were considered in this study.

Introduction

The LCLS gun design is based on the prototype gun design and includes a number of changes to improve performance. The basic modifications include improved water cooling for 120 Hz operation, dual rf feed instead of a single feed, cathode load-lock installation system, remotely operated rf tuners in both cells with positional readbacks, and symmetric probes in both cells to monitor the field level in each cell independently. This report summarizes the basic mechanical and rf properties of the prototype gun. Based on the prototype gun parameters, the LCLS specifications are also determined.

One of the biggest changes between the prototype gun and the LCLS gun is the need to operate at 120 Hz. The LCLS rf gun must operate continuously at the 120 Hz linac repetition rate with a minimum on-axis field of 120 MV/m. The prototype 1.6 cell rf gun has been operated up to 140 MV/m but only at 10 Hz. The order of magnitude increase in average power can cause thermo-mechanical distortions which may lead to changes in the rf properties of the gun such as a resonant frequency shift or a change in the stored energy per cell. As the energy is redistributed in the gun the longitudinal field profile is altered which can significantly affect the beam quality at the gun exit. Ideally the gun rf properties would be independent of the average power dissipated in the gun body so that a change to the average power would not cause a phase shift due to a frequency shift or a correlated energy spread increase due to a possible field distribution change. While in theory all relevant parameters can be measured and corrected with feedback systems, gun operation will be much simpler and more stable if the thermal effects can be eliminated or at least minimized.

This report describes the finite element thermal analysis performed on the prototype rf gun geometry using the code ANSYS. ANSYS was used to calculate the temperature distribution in the gun body and the corresponding mechanical distortions and the induced stresses [1]. ANSYS was chosen for this study because it can also

Work supported in part by the Department of Energy contract DE-AC02-76SF00515

calculate the rf parameters such as resonant frequency and field distribution. Thus the simulation was also able to calculate the change in resonant frequency and field distribution as a function of average power dissipated on the surface. The ANSYS results were used to determine the required number and location of the cooling channels.

LCLS Gun Electrical and Mechanical Specifications

A 1.6 cell, S-band, standing wave, photocathode gun was designed as part of a collaboration between BNL, SLAC and UCLA [2]. The gun was designed to produce the brightest possible electron beam with charges in the nC range. A gun based on this design is installed at the SLAC Gun Test Facility (GTF) and a drawing of the gun is shown in Figure 1. The physical dimensions of the gun are listed in Table 1.

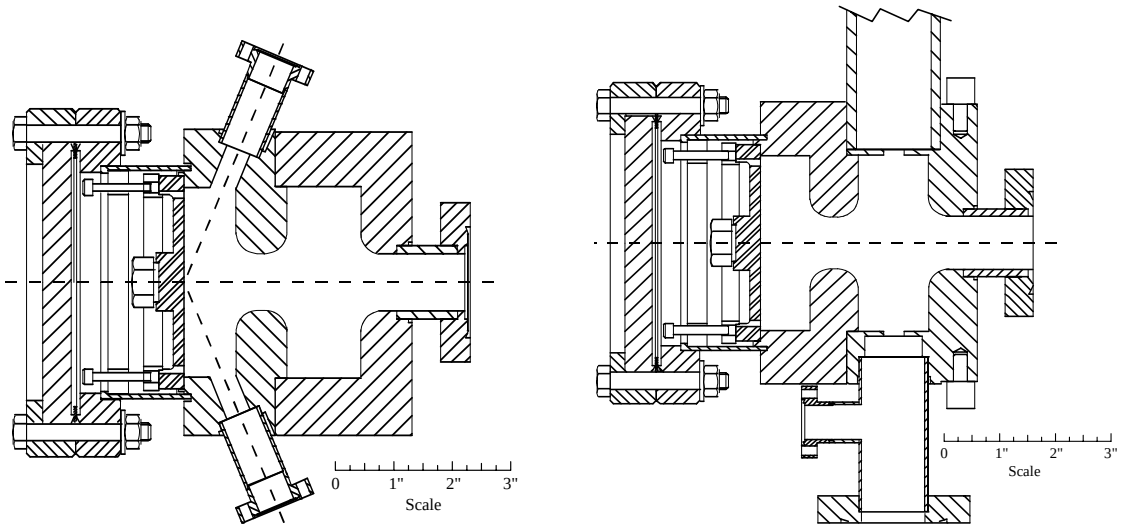

Figure 1. A drawing of the prototype1.6 cell rf gun is shown. The figure on the left shows the laser ports in the cathode cell to allow for injection of the laser beam at grazing incidence. The figure on the right is rotated 45 degrees about the beam axis to show the single rf feed and symmetric vacuum pump out port in the full cell. Not shown in the drawings are the rf tuners in the full cell. The half cell is tuned by pushing or pulling on the nut brazed on the back of the cathode plate to deflect the cathode plate longitudinally by a small amount.

Parameter	Value
Full Cell Length	3.25 cm
Full Cell Diameter	8.35 cm
Half Cell Length	2.28 cm
Half Cell Diameter	8.30 cm
Aperture Length	2.20 cm
Aperture Radius of Curvature	0.95 cm
Aperture Diameter	2.50 cm
RF Coupling Hole Size (slot length)	2.20 cm
RF Coupling Hole Size (slot width)	0.95 cm
RF Coupling Hole Thickness	0.14 cm

Table 1. Physical dimensions of the 1.6 cell prototype rf gun installed at the GTF.

The prototype gun at the GTF has been operated at 10 Hz repetition rate and up to 140 MV/m rf field on axis at a calculated average power of 0.27 kW. A similar gun with the same rf characteristics but different water cooling channel locations and sizes was designed to operate at 50 Hz [3] at an expected average power of 0.85 kW. The average power dissipated by the gun body at a given field value can be calculated from the gun shunt impedance. The shunt impedance relates the power lost on the walls to the cavity voltage. It is calculated from both the loss parameter, stored energy and the cavity Q (Quality factor relates stored energy to cavity voltage). The loss factor (relates cavity voltage to the on axis field) and stored energy (relates stored energy to the on axis field) can be calculated from simulations since they are only dependent on field distributions. The measured rf parameters for the prototype gun are listed in Table 2.

Parameter	π Mode	0 Mode
f (MHz)	2856.030	2852.525
Δf_{3dB} (MHz)	0.553	0.409
τ (ns)	576	779
$\beta = Q_0/Q_E$	1.30	1.44
Q_0	11900	11800
Q_E	9150	17000
Q_L	5160	6980
R_s (MΩ)	1.64	
k (cm)	4.8	
α (J/(MV/m)^2)	4.63 10^{-4}	

Table 2. The measured rf parameters of the LCLS prototype gun.

The average power for various repetition rates and maximum on axis field values are listed in Table 3. Power dissipation is calculated assuming a 3 μs long klystron pulse with sufficient amplitude to reach the desired field in the gun, $Q_0 = 12000$ and $\beta = 1.3$. A perfect step function excitation at 2856 MHz is assumed for the calculation. The results in table 3 only report the power dissipated in the cavity walls and do not include the reflected power. Approximately 80% of the incident power is absorbed in the gun body while the remaining 20% is reflected.

The LCLS nominal requirements are 120 MV/m on axis field and 120 Hz repetition rate. However, it is desirable to operate the gun at higher field gradients since the beam brightness increases as the field is increased. The maximum field that has been reached in the prototype gun before rf breakdown occurs is 140 MV/m. Thus the 140 MV/m, 120 Hz case, with 4 kW average power dissipation is the design goal for the LCLS gun.

Maximum Field	R = 10 Hz	R = 50 Hz	R = 120 Hz
E_c = 100 MV/m	0.17 kW	0.85 kW [3]	2.03 kW
E_c = 120 MV/m	0.25 kW		2.94 kW
E_c = 140 MV/m	0.33 kW		4.00 kW

Table 3. Average power dissipation as a function of repetition rate and peak field.

The rf frequency tuning of the prototype gun is controlled by three independent adjustments. Frequency tuning is performed in parallel with field profile measurements in order to achieve both the desired field profile and proper resonant frequency for the π mode. Each cell in the gun has a frequency tuner to allow independent control of both cells. The half cell frequency is controlled with the cathode plate position. A ½-13 threaded nut is brazed onto the back of the GTF cathode plate with a differential drive screw that is used to push or pull the cathode plate to adjust the frequency. The nut can be seen in Figure 1 although the differential screw adjustment is not shown. The GTF style half cell tuner will need modification to allow for a cathode plate load lock system. The load lock will allow for cathode replacement in a completely controlled environment to limit cathode performance degradation due to possible environmental contamination of the cathode surface. The full cell has capacitive tuners 90 degrees rotated from the rf feed and pump out port. The tuners are symmetrically located and adjusted to eliminate dipole fields. These tuners affect the stored energy in each respective cell so they also control the field level or the longitudinal gun field profile. Thus the field profile is adjusted by moving both the full cell and half cell tuners to reach the desired field profile and then the final rf frequency is adjusted by adjusting the temperature of the entire gun. The measured effect on the frequency of both modes by each tuning method is shown in Table 4.

Tuning Adjustment	π Mode	0 Mode	Units
Half cell tuning	68.3	104	kHz/mil
Full cell tuners	18	10	kHz/mil
Temperature tuning	-52.5	-52.8	kHz/C˚
Δf as pressure drops from 760-0 Torr	737	746	kHz

Table 4. The measured rf tuning parameters for both modes of the LCLS prototype gun. The positive direction for movement of both the half cell and full cell tuners is into the gun. The value for the full cell tuner assumes both tuners are moved the same direction and distance. The frequency increases approximately 750 kHz as the pressure is reduced from 760 to 0 Torr.

The LCLS gun must have several diagnostics included in order to monitor its operating parameters. The diagnostics include capacitive probes in both the full cell and half cell to independently monitor the fields in both gun cells. The probes should be built in pairs symmetrically located on each cell to eliminate dipole terms. Both the amplitude and phase of each probe is monitored to properly record the gun operating point. Position sensors on the cell tuners are also required to monitor the tuner position. In addition several thermocouples are necessary to measure the temperature of the gun. The combination of all these signals is required to determine the resonant frequency of the gun when it is in normal operation with high power. The frequencies of both modes are initially tuned at low power using a network analyzer. The frequency shift due to thermal loading at high power is difficult to measure accurately since the network analyzer can no longer be used. At the GTF the effect is estimated by measuring the amplitude and phase of the incident rf pulse and fitting the reflected power and cell probes as a function of time. One of the fit parameters is the resonant frequency and at the GTF the results of the fitting indicate that the resonant frequency drops by approximately 100 kHz with 250 W dissipated in the gun.

The specifications for the LCLS gun are shown in Table 5. The frequency is determined by the SLAC klystron frequency. All mechanical dimensions and tolerances are chosen to achieve this frequency and the desired field profile shown in Figure 2. The requirement for the maximum frequency shift from 0 to full power to be < 100 kHz is primarily due to the width of the π mode resonance (see Table 2). With larger frequency deviations the field on axis is reduced for a constant klystron power and a substantial phase shift is also encountered due to the standing wave. The variation of phase with resonant frequency is proportional to the filling time of the cavity. A 100 kHz frequency shift would produce an 18 degree phase shift for a 500 ns filling time. Larger frequency deviations would be increasingly difficult to control with feedback. This phase shift also determines the temperature stability requirement of 0.07 ˚C corresponding to 1 degree of gun phase fluctuation. The mode separation must be maintained at a minimum of 3.5 MHz for the desired field profile shown in Figure 2 in order to reduce the mode beating effects to tolerable levels. The rf coupling coefficient should be between 1.6 and 2 to reduce the filling time so that transient effects are not important with short klystron pulses of approximately 2.5 μs. However, increasing the coupling coefficient too much will significantly increase the reflected power and also require a larger coupling hole which increases the rf quadrupole field term. Therefore the maximum size of each rf coupling hole should be kept smaller than the dimensions listed in Table 1. The Q_0 of the cavity is kept large to keep the shunt impedance at a large value so significantly increased rf power is not needed to maintain the proper field level. The maximum field level desired in the gun on axis is 140 MV/m with less than 2 % deviation from the nominal field profile shown in Figure 2. The field profile is typically measured with a bead drop measurement and then compared with SUPERFISH simulation results. Due to the mechanical properties of Cu the yield strength depends on the number of braze cycles. Thus the maximum von Mises stress allowed in the Cu gun body is somewhere in the range of 3-5 ksi. Clearly the stress should be minimized to avoid plastic deformation.

Parameter	Value	units
f_π	2856.0	MHz
$f_{\pi\ 0power} - f_{\pi\ highpower}$	< 100	kHz
$f_\pi - f_0$	> 3.5	MHz
τ	450-550	ns
$\beta = Q_0/Q_E$	1.6-2	
RF Coupling holes	2	
RF coupling hole maximum area	1.91	cm^2
Q_0	>11500	
E_{max} on axis	140	MV/m
$(E-E_{nom})/ E_{nom}$ along the axis	2	%
Maximum von Mises stress	3-5	ksi
Gun Temperature Stability	0.07	˚C

Table 5. The LCLS gun electrical and mechanical specifications.

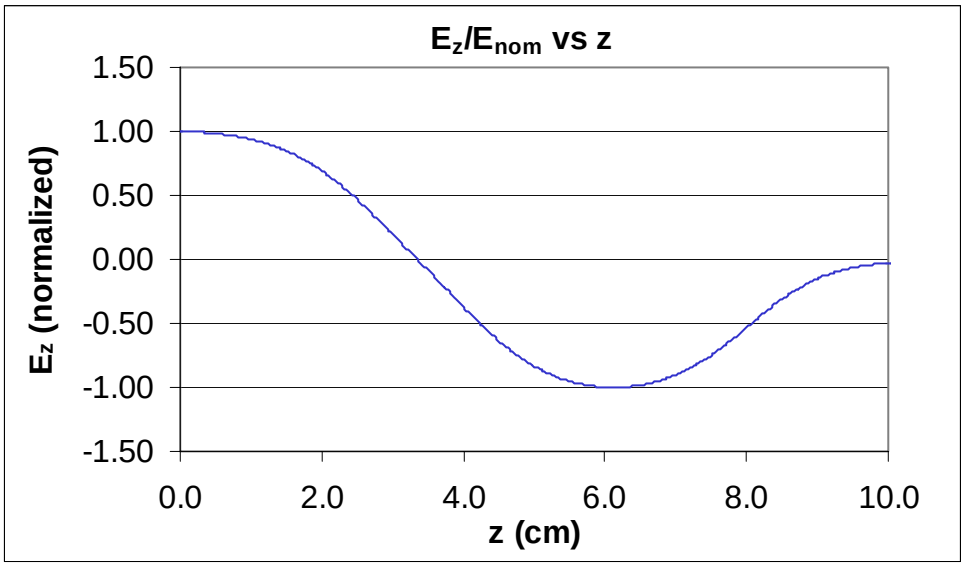

Figure 2. The normalized longitudinal electric field on axis as a function of longitudinal position is plotted for the π mode as calculated by SUPERFISH. The desired field profile has equal amplitudes in both the full and half cell.

ANSYS Modeling

SLAC has excellent resources for solving RF problems such as calculating resonant frequencies and computing the electric field in RF structures. While this may be sufficient for physics modeling of the structure it is typically not sufficient for fabricating structures in high power applications. In these cases the engineer would like to determine the RF power lost on the cavity surface and then compute the resulting thermo-mechanical distortions. The final step is to close the loop and calculate the effect of the distortions on the RF fields to determine if the structure will operate as required. The general finite element analysis program, ANSYS, was chosen for this task because it can perform all the necessary rf and mechanical computations.

Previously, thermal stress analysis for the SLAC PEP2 cavity was performed using ANSYS. In the beginning the thermal load data were entered as input to the ANSYS thermal model from another program written by Chalk River Laboratories. After high frequency electro-magnetic field elements were added to the ANSYS library, the entire calculation was performed in ANSYS. The solutions for the resonant modes and electric fields were in agreement with MAFIA. Then the solution of the magnetic *H* field was used to calculate the power loss on the surface. At first the ANSYS solution for the power loss gave a poor solution at the surface because it was based on the *H* value at the interior of the elements. An ANSYS subroutine was developed to calculate the power loss at the surface using the nodal values of *H* at the surface which then agreed with MAFIA. The calculated power lost on the surface was scaled to match the total power dissipated in the device and the heat flux distribution was then used as the input for the ANSYS thermal analysis. Finally the temperature distribution was used as the input to the ANSYS structural analysis which solved for the structure strains, stresses and displacements. The cavity distortions are then used to solve for the new rf field distribution to determine the thermal effects on the gun rf fields.

SUPERFISH vs. ANSYS Comparison

Using the PEP2 cavity work as a guide, the general ANSYS analysis methodology has been applied to the preliminary design of the LCLS gun. As described above all calculations are consolidated into a single program, ANSYS, to solve for resonant frequencies, generate a thermal load distribution, solve for thermal strain, solve for the thermal stress, and finally re-solve for the resonant frequencies of the deformed geometry.

The RF properties of the prototype gun have been studied previously with the 2D code SUPERFISH. The geometry of the prototype rf gun is shown in Figure 3 along with the rf fields as calculated by SUPERFISH. This geometry is identical to the SSRL gun except for very minor differences in the radii of the cells. A SUPERFISH input file with the gun geometry is listed in Appendix A. The initial goal was to create a simple axisymmetric model in ANSYS with identical geometry and compare results with those from SUPERFISH to validate the ANSYS RF calculations. A ¼ sector 3D model of RF elements representing the axisymmetric vacuum volume of the gun was created as shown in Figure 4. The resonant modes found in the first ANSYS run differed from those from the SUPERFISH solution by 0.5 %. However, it became obvious that the mesh size was too coarse to solve accurately for the resonant modes and electric field. After some element size refinement, the results for the resonant frequency differed by less than .01%. The electric field along the central axis and magnetic field along the cavity surface compared well with SUPERFISH as shown in Figure 5. The model was also reduced to a 1/32 sector of the full 3D model to decrease the solution time.

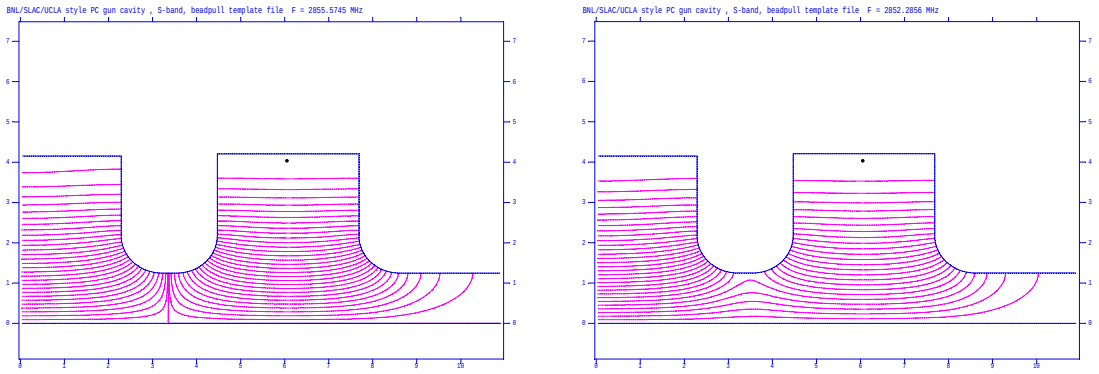

Figure 3. 2D cross-section of axisymmetric gun cavity with rf fields calculated by SUPERFISH. The π mode field distribution is on the left and the 0 mode field is on the right. The cathode is at the lower left in both figures and the gun exit is on the right.

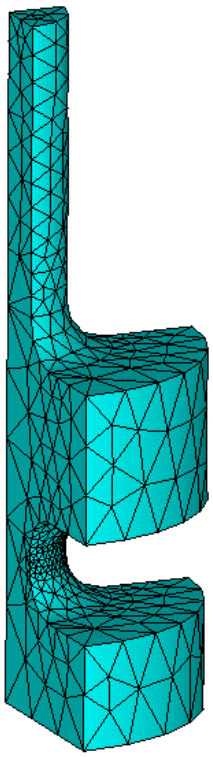

Figure 4. ¼ sector ANSYS 3D model of RF gun cavity.

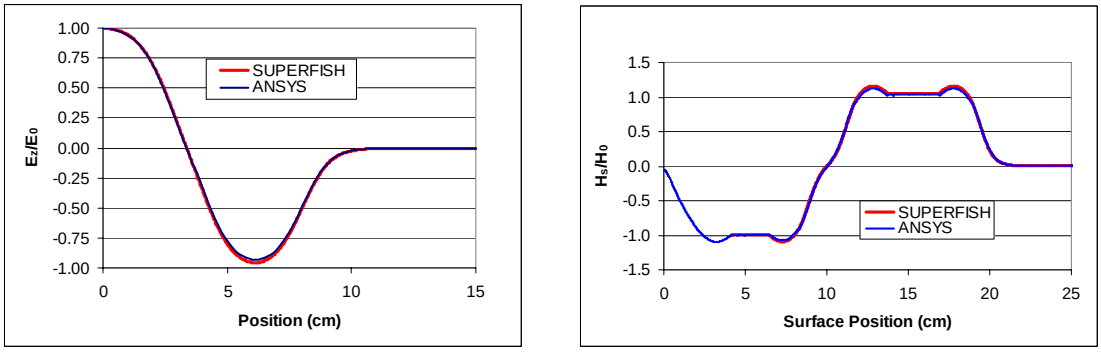

Figure 5. The plot on the left shows the longitudinal electric field on axis vs longitudinal position as calculated by both SUPERFISH and ANSYS. The plot on the right shows the magnetic field calculated by both programs as a function of position along the cavity surface. The cathode is located at 0 in both plots.

Thermal and Structural Calculations with ANSYS

With ANSYS correctly calculating the rf field distribution in the gun cavity, the copper gun body was created in the ANSYS model. One difference between the model and the prototype gun is that the model assumes there is no joint where the cathode plate meets the gun body. In the prototype gun this is a press fit and will not transfer the heat as efficiently as assumed in the model. A 1/32 sector model of the rf gun is shown in Figure 6. The two cooling channels seen in the figure are identical to the prototype gun

although the channels in the model are fully axisymmetric while the prototype is not. The transfer of heat from the copper to the water is determined by the forced heat convection coefficient, *h*. The value for *h* assumed in the calculation is 20,000 $W/m^2/C$. The water velocity is determined by solving the Dittus and Boelter equation. A velocity of 16 fps was calculated for the model parameters.

The surface power loss distribution for the surface nodes, which is proportional to H^2, was calculated using the ANSYS subroutine developed at SLAC. The model and heat flux incident on the cavity surface are shown in Figure 6. The peak heat flux is at the point of maximum surface magnetic field and agrees with the magnetic field plot in Figure 5. The incident heat flux distribution was scaled to the total steady state power loss of 3.7 kW. The steady-state temperature profile as calculated by ANSYS is shown graphically in Figure 7 with a water temperature of 20˚ C.

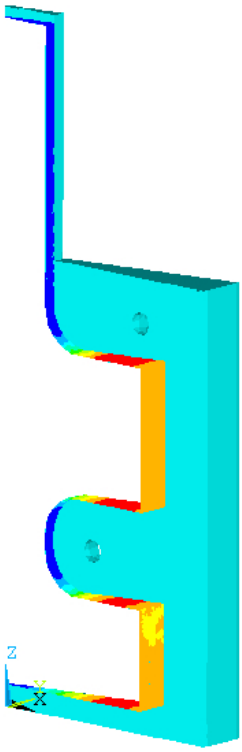

Figure 6. 1/32 sector ANSYS 3D model of RF gun body showing heat flux distribution.

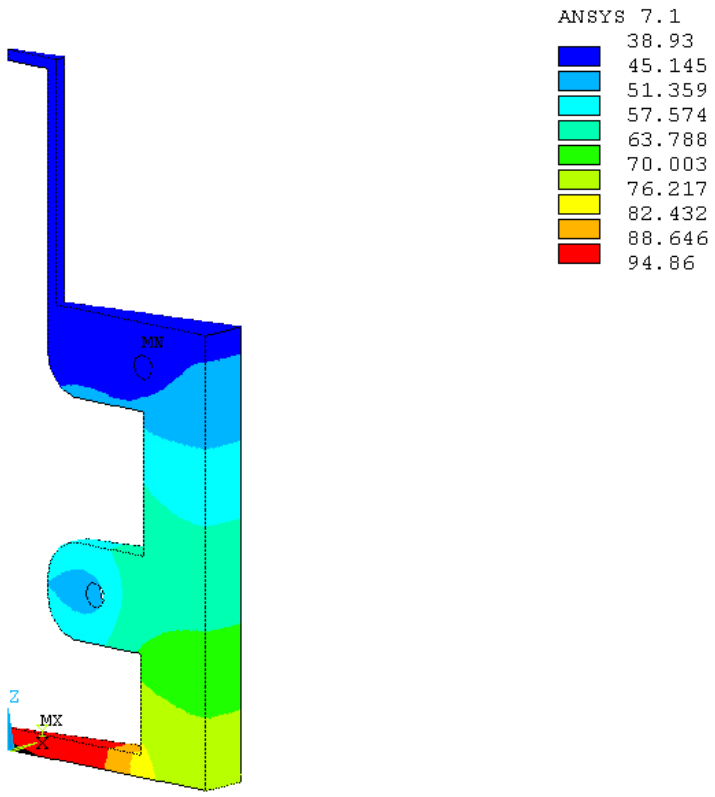

Figure 7. The temperature distribution for the model and thermal load shown in Figure 6 with 20˚ C water. The temperature scale in the upper right of the figure is in Celsius.

The subsequent structural analysis calculation in ANSYS produced the thermal deflection shown in Figure 8 and the strain shown in Figure 9 as a result of the temperature distribution in Figure 7. For the structural analysis ANSYS assumes the cathode is fixed and the rest of the gun body distorts as required due to the thermal expansion. The maximum deflection is about 100 μm. The maximum strain of .001 m/m occurs in the cathode plate where the maximum temperature gradient exists. Subsequent RF analysis with this "deformed" geometry estimated that the resonant π-mode frequency dropped by about 1750 kHz for a power loss of 3.7 kW. The frequency shift with two cooling channels yields a frequency shift over one order of magnitude larger than is acceptable so clearly some form of additional cooling will be required.

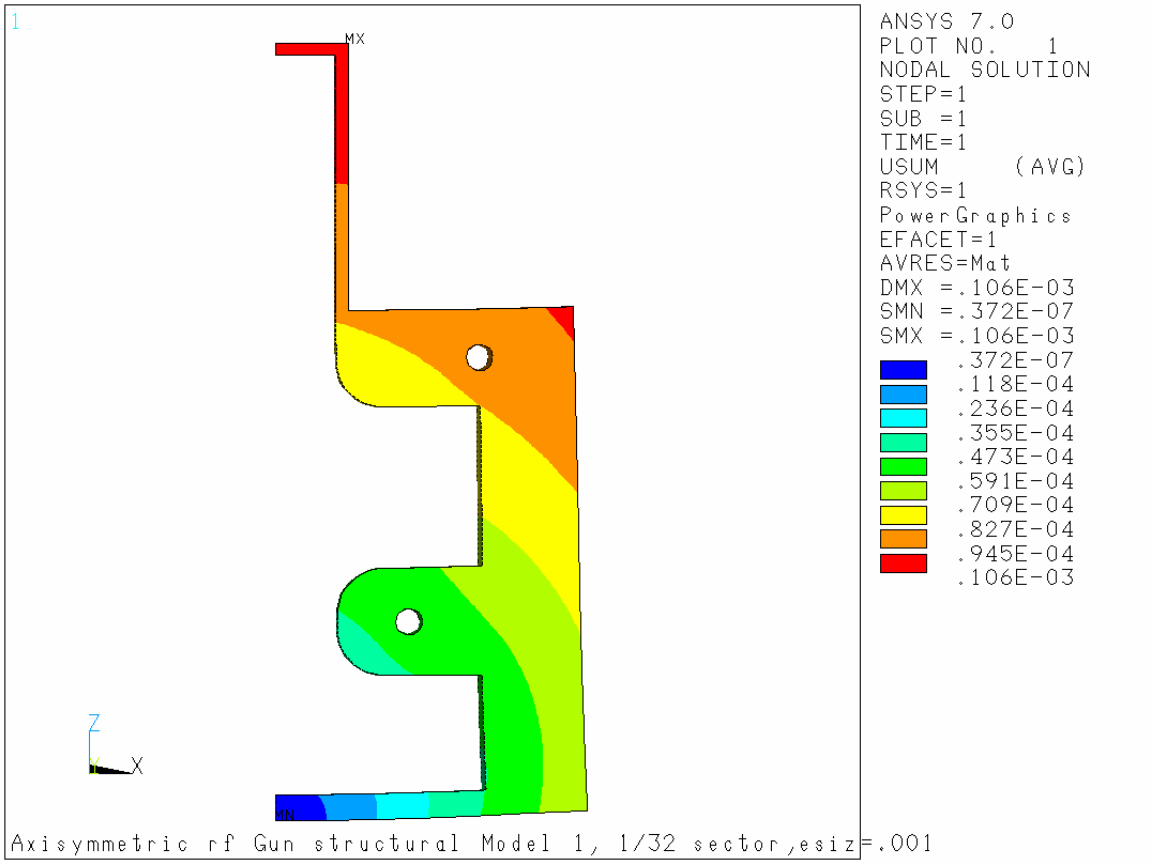

Figure 8. The total deflection in m for the thermal distribution shown in Figure 7.

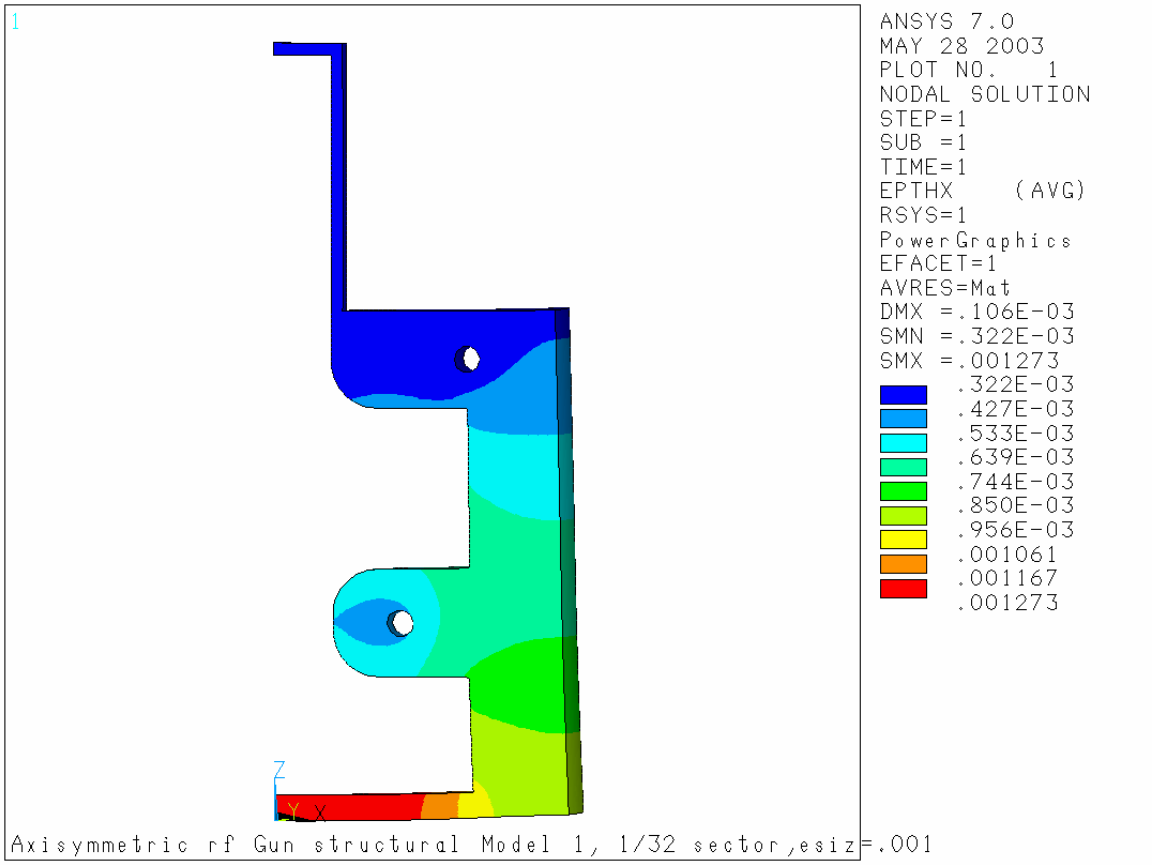

Figure 9. The total thermal strain in m/m for the thermal distribution shown in Figure 7.

Model Comparison with Prototype RF Measurements

Before using ANSYS to design the proper cooling channel locations, it seemed prudent to compare the results with measurements on the prototype gun at the GTF. Since the prototype gun cooling channels are not fully axisymmetric, the forced heat convection coefficient was modified to compensate for the different cooling channel surface area in the ANSYS model. The value for *h* was calculated for the prototype gun geometry and then scaled to the fully axisymmetric geometry in the model to produce the same heat transfer. Thus for the ANSYS calculation it was assumed h = 14,483 $W/m^2/C$ and correspondingly the water flow velocity was reduced to 11 fps.

The prototype gun is typically operated at 115 MV/m and 10 Hz repetition rate so the average power is approximately 230 W. With 230 W incident heat flux, ANSYS predicted a frequency decrease of 122 kHz due to the heating of the copper while the measured value at the GTF is a frequency drop of 50-100 kHz. The measurement is very difficult to determine within 50 kHz so the ANSYS solution is within the error bar of the measurement.

The ANSYS frequency shift vs temperature was also compared with measured values on the prototype gun. The ANSYS model predicted a 48.4 kHz decrease in π mode frequency with a 1.0° C water temperature increase and no incident heat flux. This is within 10 % of the measured value listed in Table 4.

A final verification of the model was to check the predicted stress as the water temperature was varied with no incident heat flux. Since the structure will expand uniformly with water temperature there should be no stress induced on the gun body. With a 10 °C temperature increase in the model, the change in stress was 0.0 psi. It was also confirmed that with a non-zero incident heat flux a 10° C change in the cooling water temperature would simply shift the resulting temperature distribution by 10° C. Based on the comparisons with SUPERFISH and actual measurements on the prototype gun it appears that ANSYS is correctly calculating the rf parameters, thermal distributions and the subsequent cavity distortions.

Design of Water Cooling Channels

From Figure 6 it is clear the cathode plate is roughly 80° C higher than the water temperature and the maximum strain also occurs in this region. It is obvious that the cathode plate could use an additional cooling loop. Adding a third cooling loop near the center of the cathode plate moves the hot spot from the center of the cathode to the corner of the 0.6 cell where it meets the cathode plate as shown in Figure 10. Because the temperature is uneven, the deformed shape of the model is biased such that the 0.6 cell distorts more than the full cell resulting in poor rf performance. A fourth cooling loop can be added to the gun near the new hot spot.

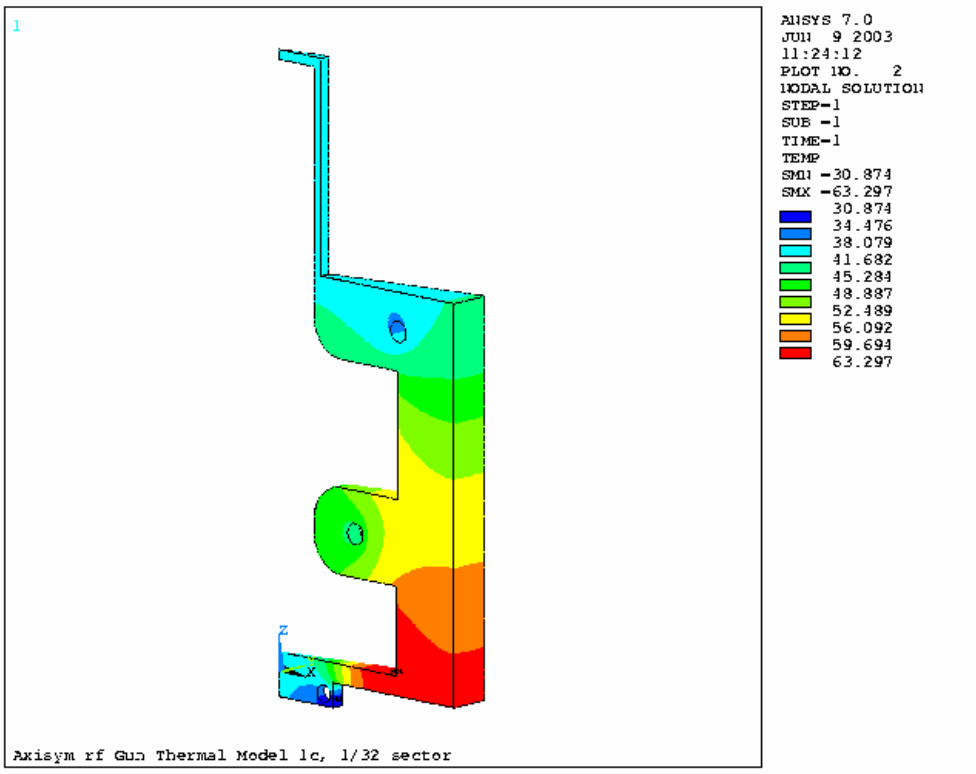

Figure 10. The temperature distribution in Celsius for the model with 3 cooling channels and 20˚ C water.

The model with four cooling channels as shown in Figure 11 has the least temperature variation of all the solutions considered so far. Since the temperature gradient is reduced the stress and resulting deformation are likewise reduced. A plot of the radial deflection is shown in Figure 12.

The resonant frequency of the gun with four cooling channels decreases 800 kHz as the power is increased from 0 to 3.7 kW. This shift is still much larger than the gun bandwidth but more than a factor of two less than the shift with only two cooling channels. However, it was determined that the frequency could be raised back to near the nominal value if the water temperature was reduced by 16° C with full power. Since the thermal gradients are causing the gun to expand nearly uniformly in the radial direction, decreasing the water temperature can shrink the gun back close to the nominal size and frequency. The cooling water temperature in the model was changed from 30° C with the rf power off down to 13.9° C with 4.0 kW average power. The resonant frequency increased 80 kHz as the power increased from zero to 4.0 kW. Thus with appropriate changes to the water temperature it is possible to keep the resonant frequency variation less than the 100 kHz specification.

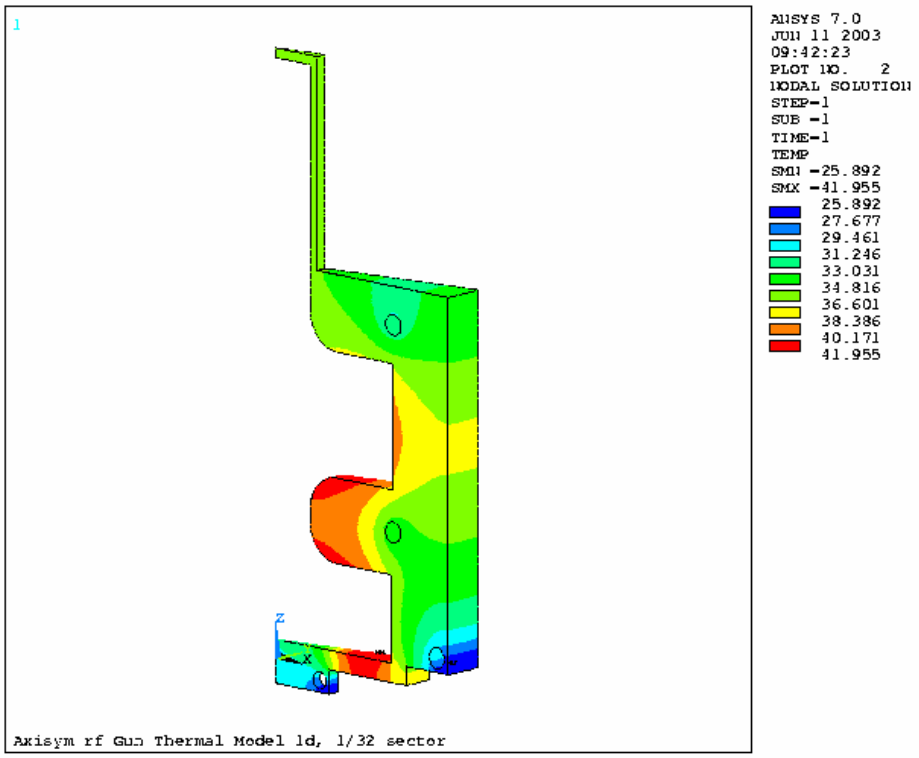

Figure 11. The temperature distribution in Celsius for the model with 4 cooling channels and 20˚ C water.

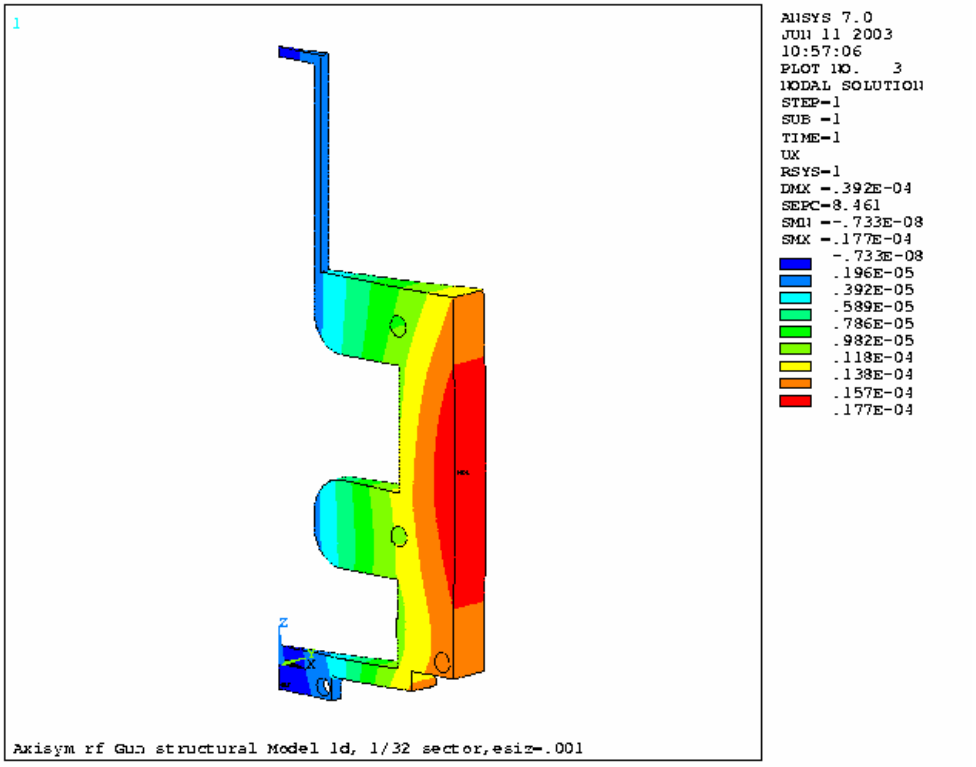

Figure 12. The radial deflection in m for the temperature distribution shown in Figure 11.

Of course it would be preferable to have the water temperature adjusted automatically so that manual adjustments are not necessary as the average rf power is varied during the course of gun operation. After examining the two thermal distributions with zero and full power, a spot on the copper body outer diameter was located where the temperature does not change significantly as shown in Figure 13. A temperature sensor located at this point could be used as the input to a feedback loop controlling the water temperature. In this manner it should be possible to maintain the gun frequency within the 100 kHz specification. This technique is used at the GTF and may explain why ANSYS overestimates the frequency shift for the 230 W case compared to the measurements.

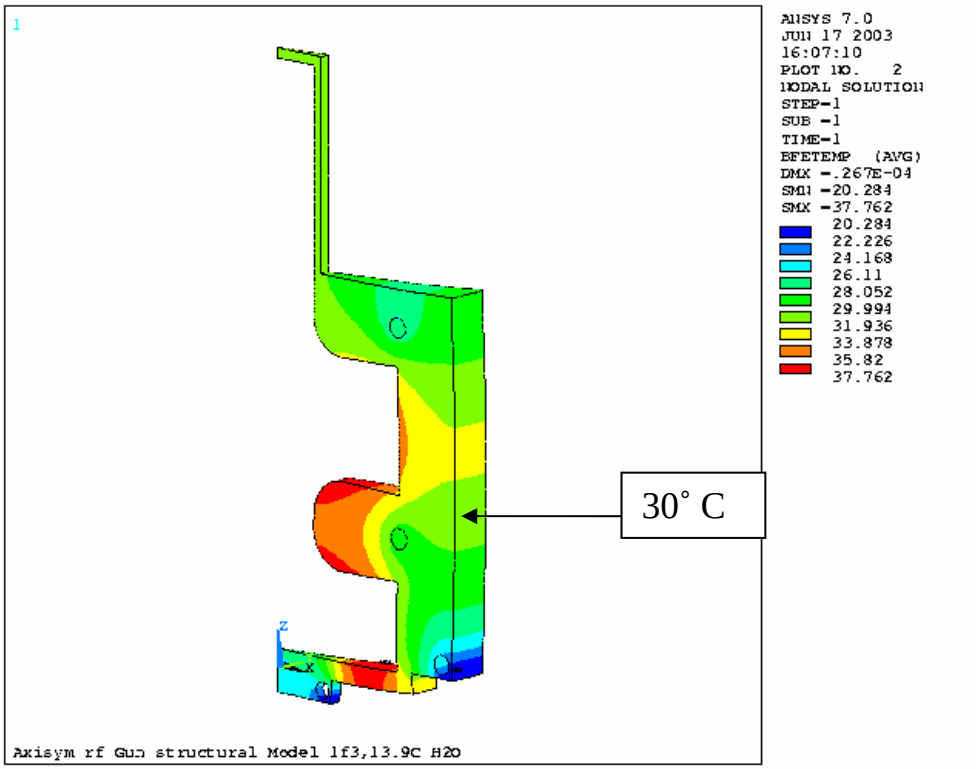

Figure 13. The temperature distribution at 4.0 kW average power input and 13.9˚ C water. The point indicated on the OD of the gun body is 30˚ C.

Gun Body Stress

In addition to the temperature distribution and its effect on rf performance, the stresses in the gun body need to be considered. The maximum allowable stress for Cu depends on the number of braze cycles and is expected to be in the range 3-5 ksi. Above these values the Cu will yield and the gun performance will likely be adversely affected. The cooling channel fabrication technique can often determine the size and potential location of the cooling channels which will strongly affect the stresses since they arise from temperature gradients. The cooling channels in the prototype gun are made by drilling straight holes in the gun body and plugging the ends where necessary. This construction has a number of disadvantages: the cooling is not axisymmetric; the water flow has a lot of sharp turns in the flow path; and most significantly, the cooling

channels cross braze joints that extend to the vacuum volume. One way to avoid these drawbacks is to move the cooling passages to the outside of the gun body and braze a hollow conductor onto the gun body after machining. The advantages of this construction are that the water circuit would not affect any other braze joints and the passage would be smooth and uniform.

This concept was modeled with ANSYS with two sizes of water passages: 3.2 and 4.8 mm diameter. The results showed that the differences in the cooling passage size had a very small effect on the stress in the copper but the placement of the passages at the outer diameter of the gun body caused more than a factor of two increase in the gun body stresses as shown in Table 6. The gun body stresses are shown in Figure 14 for both sizes of water passage. The case with four cooling channels inside the gun body is the only case that is close to the desired maximum stress level.

Channels	Channel Diameter	Location	Max Stress
2	5.6 mm	Inside Gun Body	6.7 ksi
3	5.6 mm	Inside Gun Body	5.3 ksi
4	5.6 mm	Inside Gun Body	3.3 ksi
4	3.2 mm	Around Gun OD	7.0 ksi
4	4.8 mm	Around Gun OD	6.8 ksi

Table 6. The maximum stress in the gun body for the various water cooling schemes simulated with ANSYS assuming 3.7 kW average power dissipation in the cavity walls.

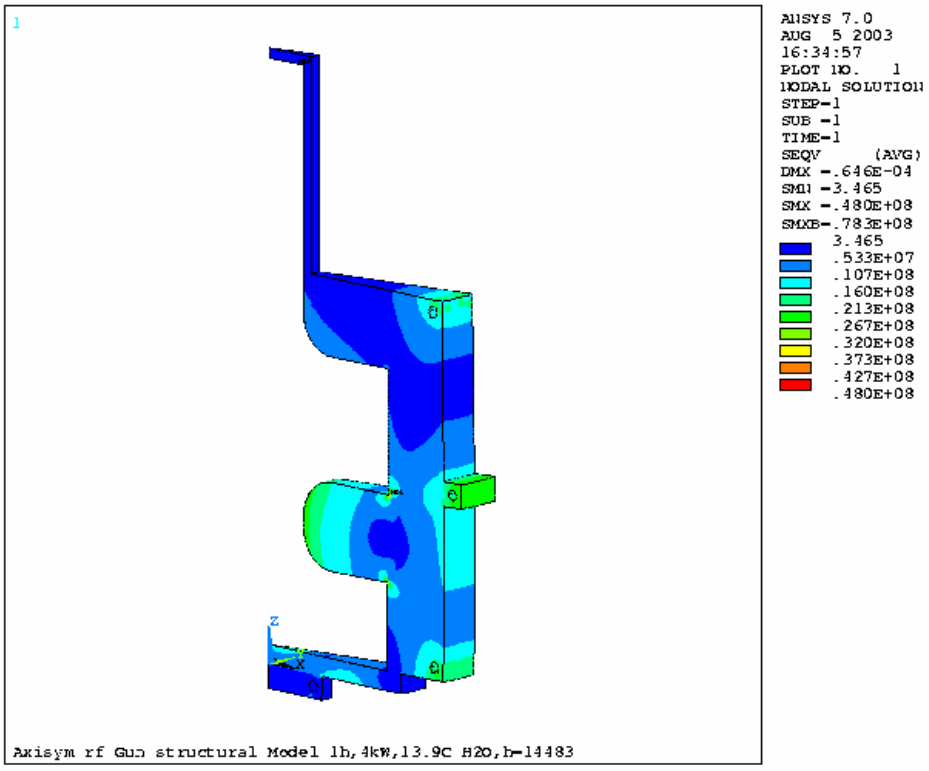

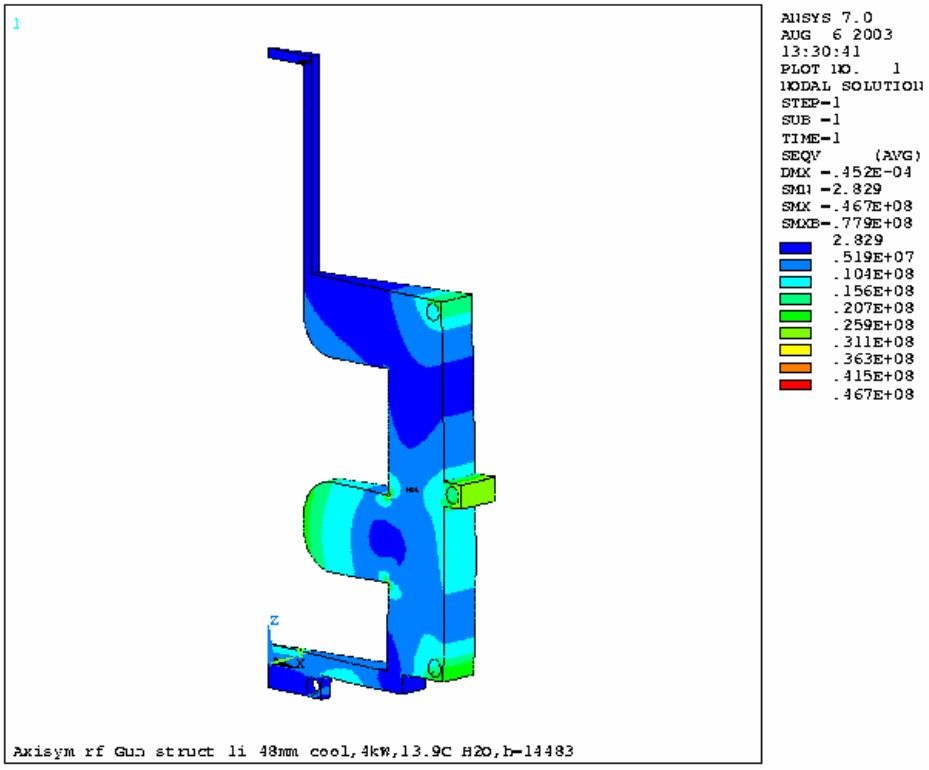

Figure 14. Gun body stresses in Pa with water cooling passages moved to the gun body outer diameter. The upper plot has 3.2 mm diameter water passages and the lower plot uses 4.8 mm diameter water passages.

The maximum stress with the water passages at the gun OD was 6.8 ksi for the case with 4.8 mm diameter channels. This is larger than maximum allowable von Mises stress of 5 ksi listed in Table 5. Thus this technique was rejected in favor of the cooling channel machined inside the gun body. Additional work is necessary to determine the proper method of gun fabrication in order to achieve axisymmetric cooling channels.

3D Gun Model with RF Aperture Analysis

A 3D ANSYS model was constructed to examine the heating of the gun at the rf apertures. The model is similar to the prototype RF gun and includes the correct iris dimensions. The prototype gun has only one rf aperture, but the LCLS will use two apertures. The ANSYS model includes two apertures because it is constructed from a 90-degree sector. The 3D ANSYS model included only two cooling channels as the primary focus of the 3D study was the rf aperture. Since the two additional cooling channels are near the cathode plate and far from the aperture they were not considered important to determine the temperature and stresses at the aperture.

ANSYS predicted a π-mode resonance of 2862 MHz compared with 2856 MHz with the 2D model. In the 3D model the cell dimensions are smaller in radius by 13 mils in the full cell and 3 mils in the half cell. The ratio of peak full cell field to half cell is 0.903 compared to 0.932 with the 2D model. The maximum heat flux at the aperture is 1.1 W/mm^2. The maximum temperature at the aperture is about 72° C and the maximum von Mises stress of 14 kPSI occurs on the side of the aperture at its thinnest point. This stress level significantly exceeds the maximum stress listed in Table 5. Figures 15 and 16 show the temperature and stress distributions respectively for the 3D case.

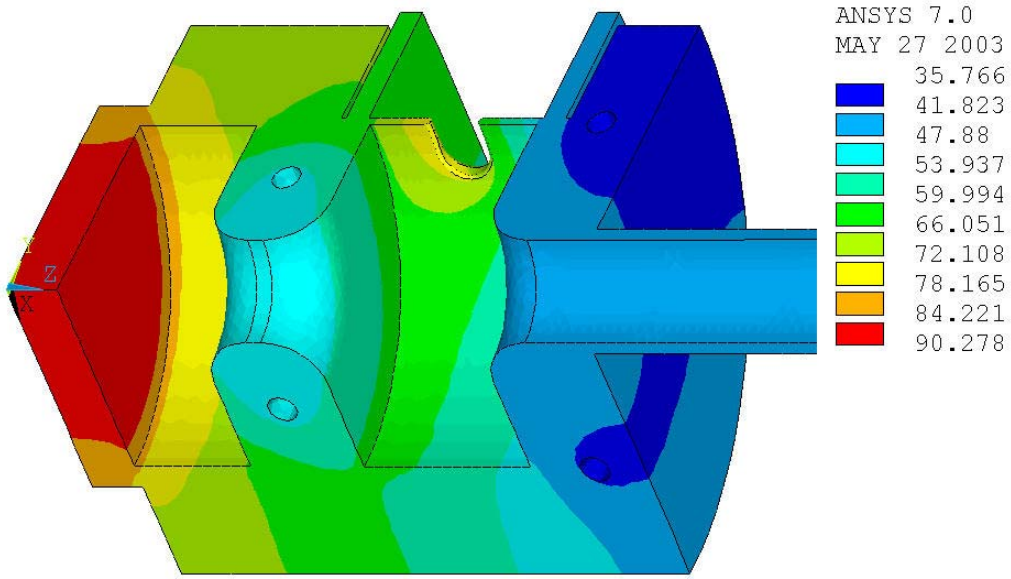

Figure 15. Gun body temperature distribution for the 3D model with 2 water cooling channels and 20° C water.

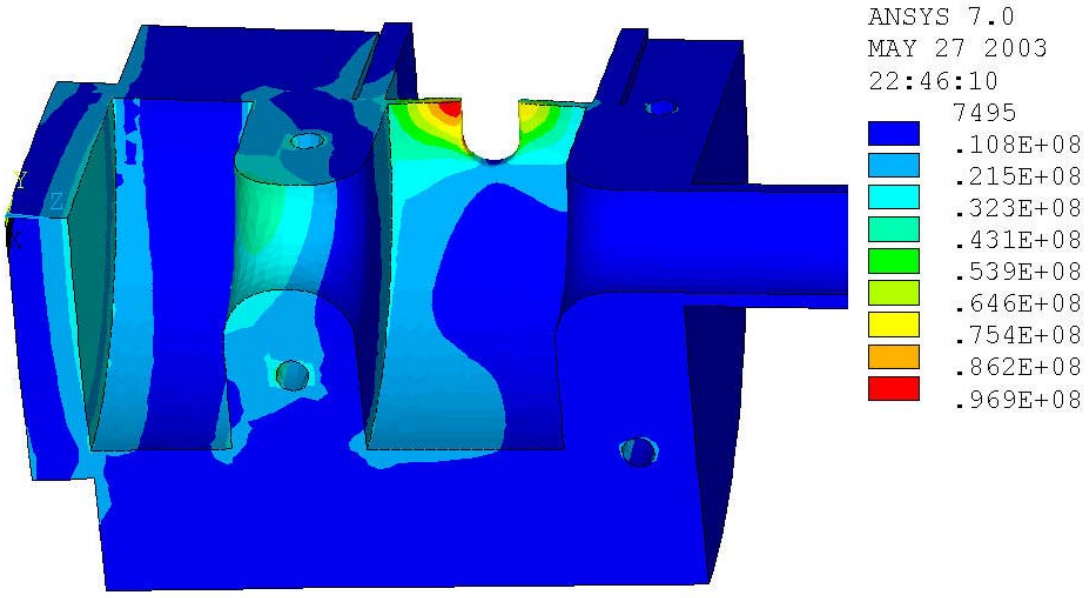

Figure 16. Gun body stress in Pa for the temperature distribution shown in Figure 15. The maximum stress of 14 ksi occurs around the rf aperture.

A second 3D model was constructed with the aperture thickness doubled at the thinnest point. The results for this model are a π-mode frequency of 2863 MHz, *E* field full cell to half cell ratio of 1.18, maximum iris heat flux of 0.9 W/mm^2, maximum iris temperature of about 71° C, and a maximum von Mises stress of 11 ksi.

The second model has a rather different *E* field shape and the temperature of the cathode has dropped from 90 to 80 °C due to the change in field distribution. Thus a third 3D model was constructed reducing the length of the half cell by 9 mils to rebalance the field distribution. The results for this model are a π-mode frequency of 2863 MHz, *E* field ratio of 0.898, maximum iris heat flux of 0.7 W/mm^2, maximum iris temperature of about 72 °C, and a maximum von Mises stress of 10 ksi. The cathode temperature agreed very well with the first model because the field distribution was nearly identical.

The decrease in stress is smaller than the factor of two that was used to increase the thickness. However, the point of maximum stress has now moved from the thinnest part of the aperture in the middle of the straight section (as shown in Figure 16) to the end of the aperture where it is curved. When the thinnest part of the aperture is doubled in thickness, the ends are only increased by 50%. The reduction in stress was 71% compared to an expected 67% reduction in stress assuming the stress varies inversely with the thickness at the aperture end. If the stress continues to scale inversely with the aperture thickness at the ends, it would require an aperture over 1 cm thick to reduce the stress to the 3 ksi level.

Clearly additional work on the rf aperture is still required to reduce the stress. It is also clear that changing the aperture thickness will decrease the rf coupling. However, the rf coupling needs to be reduced because the addition of a second rf aperture of identical size will double the prototype gun coupling coefficient from 1.3 to 2.6. Thus some decrease in size or increase in thickness will be required to get the desired coupling coefficient of 1.6-2. An increase in aperture thickness will decrease

the stress but decreasing the aperture size should increase the stress. Introducing a small taper on the waveguide side of the aperture may help reduce the stress by increasing the volume of Cu as one moves away from the aperture edge without affecting the coupling coefficient since the Cu thickness at the aperture edge would be unchanged. This idea has not yet been studied. The addition of a second aperture will also increase the rf quadrupole field component. Ideally the size of the apertures would be reduced so that the total quadrupole field is no larger than the component from a single rf feed in the prototype gun.

Finally the pulsed heating effects, especially on the rf feed apertures, must be considered. The fact that the prototype gun or others like it around the world have not exhibited any failures at the aperture is encouraging. Of course the 120 Hz LCLS repetition rate and minimum 120 MV/m field strength will cause the gun to age more than 12 times faster than the prototype gun.

Conclusions

The LCLS gun will be similar to the prototype gun at the SLAC GTF. The basic modifications include improved water cooling for 120 Hz operation, dual rf feed instead of a single feed, cathode load-lock installation system, remotely operated rf tuners in both cells with positional readbacks, and symmetric probes in both cells to monitor the field level in each cell independently. The complete LCLS gun specifications are listed in Table 5.

After studying the thermo-mechanical properties of the LCLS rf gun with ANSYS there are some general trends that are evident in studying the results of the analysis. First, there is less stress in the gun body due to the RF heating of the copper if the cooling channels are closer to the centerline of the gun. With the cooling channels closer to the heat source, there is a reduction of the absolute temperature and the temperature gradients. Stresses in the copper are due to the temperature gradient and not the absolute temperature as long as the gun is fabricated from one material. Since the stress is proportional to the temperature gradient, the stress is proportional to the incident power.

It appears that with four cooling channels located as shown in Figure 13 keeps the thermal gradients to sufficiently low levels that the stress just barely exceeds the specification. Since changing the temperature of the copper body does not change the stress, frequency tuning with water temperature is acceptable just as in other rf structures. According to ANSYS there is a point on the OD of the gun body that does not change temperature as the incident power is increased and the water temperature is decreased to keep the resonant frequency constant. Thus a temperature sensor could be located at this point and used in a feedback loop to keep the gun frequency relatively constant. According to simulations it will vary by less than the 100 kHz specification as the power is varied from zero to 3.7 kW.

The RF feed on the prototype gun has been tested to approximately 0.33 kW of average power. The LCLS gun is expected to run at 4 kW of average power. The 14 ksi stress at the aperture greatly exceeds the maximum allowable stress for Cu. Further study is required to determine the proper aperture size and thickness needed to reduce stress at the aperture to an acceptable value, produce the desired rf coupling coefficient and minimize the rf quadrupole field component.

The thermo-mechanical study presented in this report only considers the steady state gun operation and does not consider any pulsed heating effects. Additional study is necessary to consider the pulsed heating effects on the gun performance. To date the prototype gun has never exhibited any known adverse effects due to the pulsed heating. However, the LCLS gun operates at 12 times the repetition rate so the gun will age much faster and any additional stresses due to the pulsed heating may become prohibitive.

According to ANSYS it appears the rf gun can be operated very close to specification at nearly 4 kW average power with a proper redesign of the rf aperture. However, should the gun not perform according to simulation, there is an alternative plan to reduce the average heat flux incident on the gun while still maintaining the same rf fields in the gun. Utilizing rf pulse shaping technology allows the fields to reach steady state faster and thus dissipate less power on the cavity walls [4]. This technique can reduce the average power over a factor of two and close to a factor of three. Some combination of water cooling and rf pulse shaping may be required to operate the LCLS gun.

APPENDIX A

Gun0mil.txt

```
RF GUN
&reg xmax=15.0, ymax=4.208300,freq=2856.,dx=.05,mat=1,
        xdri=6.11,ydri=4.208300,nbslf=1,
 NPEG=20, rmass=0.511 &
 &PO X=0.00,Y=0.000 &
 &PO X=0.00,Y=1.000 &
 &PO X=0.00,Y=2.000 &
 &PO X=0.00,Y=3.000 &
 &PO X=0.000,Y=4.000 &
 &PO X=0.000,Y=4.15860 &
 &PO X=2.27584,Y=4.15860 &
 &PO X=2.27584,Y=2.20218 &
 &PO NT=2,X0=3.22834,Y0=2.20218,R=0.9525,THETA=270.0 &
 &PO X=3.2766,Y=1.24968 &
 &PO X=3.3782,Y=1.24968 &
 &PO X=3.4798,Y=1.24968 &
 &PO X=3.52806,Y=1.24968 &
 &PO NT=2,X0=3.52806,Y0=2.20218,R=0.9525,THETA=0.0 &
 &PO X=4.48056,Y=4.208300 &
 &PO X=7.73176,Y=4.208300 &
 &PO X=7.73176,Y=2.20218 &
 &PO NT=2,X0=8.68426,Y0=2.20218,R=0.9525,THETA=270.0 &
 &PO X=9.62406,Y=1.24968 &
 &PO X=15.0000,Y=1.24968 &
 &PO X=15.0000,Y=0.0000 &
 &PO X=0.00,Y=0.0 &
```

Geometry input for SUPERFISH model – 2D cross-section of gun cavity.

REFERENCES

[1] I.S. Lehrman, I.A. Birnbaum, S.Z. Fixler, R.L. Heuer, S. Siddiqi, E. Sheedy, I. Ben-Zvi, K. Batchelor, J.C. Gallardo, H.G. Kirk, T. Srinivasan-Rao and G.D. Warren, *Nucl. Instr. Meth. A* **318**, 247 (1992).

[2] D.T. Palmer, "The Next Generation Photoinjector", Stanford University Thesis.

[3] F. Sakai, X. Wang, H. Kotaki, K. Nakajima, T. Watanabe, K. Kinoshita, S. Kondo, M. Kando, H. Dewa, T. Ueda, K. Yoshii, M. Uesaka, A. Ogata, H. Naanishi, M. Washio, A. Endo, I. Ben-Zvi, J. Skaritka and M. Woodle, BNL Report 65003, (1997).

[4] J.F. Schmerge, LCLS Tech note, LCLS-TN-02-7, (2002).